ORIGINAL PAPER

Extended MHD Modelling with the Ten-Moment Equations

Ammar H. Hakim

Abstract High-order moment fluid equations for simulation of plasmas are presented. The ten-moment equations are a two-fluid model in which time dependent equations are used to advance the pressure tensor. With the inclusion of the full pressure tensor Finite Larmor Radius (FLR) effects are captured. Further, Hall-effects are captured correctly by including the full electron momentum equation. Hall and FLR effects are important to understand stability of compact toroids like Field Reversed Configurations (FRCs) and also to detailed understanding of small scale instabilities in current carrying plasmas. The effects of collisions are discussed. Solutions to a Riemann problem for the ten-moment equations are presented. The ten-moment equations show complex dispersive solutions which come about from the source terms. The model is validated with the GEM fast magnetic reconnection challenge problem.

Keywords Magnetohydrodynamics (MHD) · Moment equations · Magnetic reconnection · Ten-moment equations · Two-fluid physics · Hall effects · Finite-Larmor Radius effects

Introduction

Fluid equations are a common tool to study bulk plasma behaviour. Among the most commonly used fluid models are the Magnetohydrodynamics (MHD) model [4] and the Hall-MHD model. In MHD the plasma is treated as a *single*

A. H. Hakim (✉)
Tech-X Corporation, 5621, Arapahoe Avenue Suite A, Boulder, CO 80303, USA
e-mail: ammar@txcorp.com

electrically conducting fluid. Although in the Hall-MHD model a distinction is made between the bulk plasma velocity and electron velocity, electron inertia and displacement currents are ignored and the electron and ion number-densities are assumed to be the same (quasi-neutrality). A more general approach is to treat to the plasma as a mixture of multiple fluid species. In these *two-fluid* models each plasma species is described by a set of fluid equations evolving under electromagnetic forces and collisions. The electromagnetic fields are modeled using Maxwell equations of electromagnetism. Two-fluid models retain both electron inertia effects and displacement currents and allow for ion and electron demagnetization. Further, by retaining sufficient moments of the kinetic equation, the two-fluid model can also describe Finite-Larmor Radius (FLR) effects, important when characteristic scales in the plasma are comparable to the ion gyroradius. In fusion devices, specially for Innovative Confinement Concept (ICC) devices like Field-Reversed Configurations (FRCs), there are two important spatial scales and corresponding physics effects: the ion skin-depth and the ion Larmor radius. The former describes Hall-Effects and is dependent only on the number density of the fluid. The latter describes FLR effects and depends on both the plasma temperature and magnetic fields. The Hall-MHD model, and a previously studied two-fluid model [5], captures the ion skin-depth effects but not the FLR effects. By including the pressure tensor in the fluid equations FLR effects can also be captured. The FLR effects are important to explain experimentally observed FRC stability, not explainable in the ideal MHD model. In this paper initial results of using high-order moment fluid equations to correctly capture FLR effects are described. The model used retains equations to evolve the full pressure tensor but ignores heat transfer and collisional

relaxation of the fluids. Including these effects are part of ongoing research and will be addressed in future publications.

The rest of the paper is organized as follows. First, the ten-moment equations are derived and effects of collisions discussed. Next, a Riemann problem for the ten-moment equations is formulated and numerical results presented. Although artificial from a physical perspective, Riemann problems are important mathematically as they clearly show the wave structure of the equations used. An application of the model to fast magnetic reconnection is then presented. Results from the ten-moment reconnection agree well with published results with full particle-in-cell (PIC) codes results and two-fluid results [5]. Finally, some conclusions are presented and directions for future research are outlined.

Ten-Moment Equations

Each species in a multi-component plasma is described by the Boltzmann equation which describes the temporal evolution of the particle distribution function in a six dimensional spatial and velocity space and evolves under the influence of collisions and electromagnetic forces. With the distribution function $f(\mathbf{x},\mathbf{v},t)$ defined such that $f(\mathbf{x},\mathbf{v},t)d\mathbf{x}d\mathbf{v}$ is the number of particles located in a phase-space volume element $d\mathbf{x}d\mathbf{v}$, the Boltzmann equation may be written as

$$\frac{\partial f}{\partial t} + v_j \frac{\partial f}{\partial x_j} + \frac{q}{m}(E_j + \epsilon_{kmj}v_kB_m)\frac{\partial f}{\partial v_j} = \left(\frac{\partial f}{\partial t}\right)_c. \tag{1}$$

Here $\mathbf{E}$ is the electric field, $\mathbf{B}$ is the magnetic flux density, q and m are the charge and mass of the plasma species and ε_{kmj} is the completely anti-symmetric pseudo-tensor which is defined to be ±1 for even/odd permutations of (1,2,3) and zero otherwise. Summation over repeated indices is assumed. The collision terms are represented by $(\partial f/\partial t)_c$ the exact form of which is specified later in the paper. The electromagnetic field is determined using Maxwell equations of electromagnetism

$$\nabla \times \mathbf{E} = -\frac{\partial \mathbf{B}}{\partial t} \tag{2}$$

$$\nabla \times \mathbf{B} = \mu_0 \mathbf{J} + \frac{1}{c^2}\frac{\partial \mathbf{E}}{\partial t} \tag{3}$$

$$\nabla \cdot \mathbf{E} = \frac{\varrho_c}{\varepsilon_0} \tag{4}$$

$$\nabla \cdot \mathbf{B} = 0. \tag{5}$$

Here μ_0 and ε_0 are the permeability and permittivity of free space, $c = (\mu_0\varepsilon_0)^{-1/2}$ is the speed of light and ϱ_c and $\mathbf{J}$ are the charge density and the current density defined by

$$\varrho_c \equiv \sum qn \tag{6}$$

$$\mathbf{J} \equiv \sum qn\mathbf{u}. \tag{7}$$

The summations in Eqs. 6 and 7 are over all species present in the plasma. The number density $n(\mathbf{x},t)$ and mean velocity $\mathbf{u}(\mathbf{x},t)$ are defined by

$$n \equiv \int fd\mathbf{v} \tag{8}$$

$$u_j \equiv \frac{1}{n}\int v_j fd\mathbf{v}, \tag{9}$$

where $d\mathbf{v} = dv_1dv_2dv_3$ represents a volume element in velocity space.

A simple method to obtain fluid equations is to multiply the Boltzmann equation in turn by tensors defined by products of the velocities and integrate over the velocity space. For example, in addition to the number density and mean velocities defined by Eqs. (8) and (9) the following higher order moments are defined.

$$\mathcal{P}_{ij} \equiv m \int v_i v_j fd\mathbf{v} \tag{10}$$

$$\mathcal{Q}_{ijk} \equiv m \int v_i v_j v_k fd\mathbf{v} \tag{11}$$

$$\mathcal{K}_{ijkl} \equiv m \int v_i v_j v_k v_l fd\mathbf{v}. \tag{12}$$

These definitions are most convenient to derive the moment equations although they do not have a convenient physical interpretation. In classical fluid mechanics the following physically more relevant definition are used.

$$P_{ij} \equiv m \int (v_i - u_i)(v_j - u_j)fd\mathbf{v} \tag{13}$$

$$Q_{ijk} \equiv m \int (v_i - u_i)(v_j - u_j)(v_k - u_k)fd\mathbf{v} \tag{14}$$

$$K_{ijkl} \equiv m \int (v_i - u_i)(v_j - u_j)(v_k - u_k)(v_l - u_l)fd\mathbf{v}. \tag{15}$$

The fluid equations displayed below suggest, for example, interpreting P_{ij} as a fluid stress tensor and Q_{ijk} as a heat flow tensor. As is easily shown, the moment set Eqs. 10–12 and Eqs. 13–15 are related by

$$\mathcal{P}_{ij} = P_{ij} + nmu_i u_j \tag{16}$$

$$\mathcal{Q}_{ijk} = Q_{ijk} + u_{[i}\mathcal{P}_{jk]} - 2nmu_i u_j u_k \tag{17}$$

$$\mathcal{K}_{ijkl} = K_{ijkl} + u_{[i}\mathcal{Q}_{jkl]} - u_{[i}u_j\mathcal{P}_{kl]} + 3nmu_i u_j u_k u_l. \tag{18}$$

In these equations square brackets around indices represent the minimal sum over permutations of free indices needed to yield completely symmetric tensors. For example $u_{[j}\mathcal{P}_{ik]} = u_j\mathcal{P}_{ik} + u_i\mathcal{P}_{kj} + u_k\mathcal{P}_{ji}$.

Using this procedure leads to the set of *exact* moment equations listed below

$$\frac{\partial n}{\partial t} + \frac{\partial}{\partial x_j}(nu_j) = 0 \tag{19}$$

$$m\frac{\partial}{\partial t}(nu_i) + \frac{\partial \mathcal{P}_{ij}}{\partial x_j} = nq(E_i + \epsilon_{ijk}u_j B_k) + R_c \tag{20}$$

$$\frac{\partial \mathcal{P}_{ij}}{\partial t} + \frac{\partial \mathcal{Q}_{ijk}}{\partial x_k} = nqu_{[i}E_{j]} + \frac{q}{m}\epsilon_{[ikl}\mathcal{P}_{kj]}B_l + P_c \tag{21}$$

$$\frac{\partial \mathcal{Q}_{ijk}}{\partial t} + \frac{\partial \mathcal{K}_{ijkl}}{\partial x_l} = \frac{q}{m}(E_{[i}\mathcal{P}_{jk]} + \epsilon_{[ilm}\mathcal{Q}_{ljk]}B_m) + Q_c \tag{22}$$

In these equations R_c, P_c and Q_c are yet unspecified terms arising from the collision operator in the Boltzmann equation. Equations 19–22 are 20 equations $(1 + 3 + 6 + 10)$ for 35 unknowns ($\mathcal{K}_{ijkl}$ has 15 independent components). In general any finite set of exact moment equations will always contain more unknowns than equations. To reduce the number of unknowns and make the system determinate closure relations must be employed. Deriving accurate closure relations is difficult and an extensive set of closures relevant to various physical situations are known. In this paper we presently circumvent the problem by assuming that the divergence of the heat flux tensor $Q_{ijk,k}$ vanishes. Although this may be an inaccurate assumption for certain physical situations, the numerical methods used here are easily adapted to handle general closure relations by including them as additional source terms in the fluid equations. Note that a non-zero pressure tensor, but a vanishing heat flux tensor, is equivalent to assuming that the distribution function is a Gaussian

$$\mathcal{G} = \frac{n}{(2\pi)^{3/2}\Delta^{1/2}}\exp\left(-\frac{1}{2}\Theta_{ij}^{-1}c_i c_j\right) \tag{23}$$

where, $\Delta = \det(\Theta_{ij})$, $\Theta_{ij} = P_{ij}/mn$ and $c_i = v_i - u_i$. In previous analysis to compute closures for the pressure tensor the distribution function is expanded in inverse mean-free path around a Maxwellian. As is easily shown this distribution function expansion about a Maxwellian does not allow

arbitrary anisotropy in the pressure tensor as the distribution function is no longer always non–negative. On the other hand the Gaussian shown above is always non–negative, as for $\Delta > 0$ and $n > 0$ the matrix Θ_{ij} is positive definite and remains so under the flow. Closure analysis, if carried out by expanding the distribution around the Gaussian Eq. (23), will lead to, in general, more accurate relations for the heat-flow tensor.

The set of fluid equations is called a *two-fluid ten-moment model* or a *ten-moment* model for short. For a two species plasma it has $2 \times 10 + 6 = 26$ equations. In one dimension and in Cartesian coordinates identifying the subscripts $(1,2,3) \equiv (x,y,z)$, these equations are put into the conservation law form

$$\frac{\partial \mathbf{q}}{\partial t} + \frac{\partial \mathbf{f}}{\partial x} = \mathbf{s}, \tag{24}$$

where the conserved variables and fluxes are

$$\mathbf{q} = \begin{pmatrix} \rho \\ \rho u \\ \rho v \\ \rho w \\ \rho u^2 + P_{xx} \\ \rho uv + P_{xy} \\ \rho uw + P_{xz} \\ \rho v^2 + P_{yy} \\ \rho vw + P_{yz} \\ \rho w^2 + P_{zz} \end{pmatrix}, \mathbf{f} = \begin{pmatrix} \rho u \\ \rho u^2 + P_{xx} \\ \rho uv + P_{xy} \\ \rho uw + P_{xz} \\ \rho u^3 + 3uP_{xx} \\ \rho u^2 v + 2uP_{xy} + vP_{xx} \\ \rho u^2 w + 2uP_{xz} + wP_{xx} \\ \rho uv^2 + uP_{yy} + 2vP_{xy} \\ \rho uvw + uP_{yz} + vP_{xz} + wP_{xy} \\ \rho uw^2 + uP_{zz} + 2wP_{xz} \end{pmatrix} \tag{25}$$

and sources are

$$\mathbf{s} = \begin{pmatrix} 0 \\ r\rho(E_x + vB_z - wB_y) \\ r\rho(E_y + wB_x - uB_z) \\ r\rho(E_z + uB_y - vB_x) \\ 2r\rho uE_x + 2r(B_z\mathcal{P}_{xy} - B_y\mathcal{P}_{xz}) \\ r\rho(uE_y + vE_x) + r(B_z\mathcal{P}_{yy} - B_y\mathcal{P}_{yz} - B_z\mathcal{P}_{xx} + B_x\mathcal{P}_{xz}) \\ r\rho(uE_z + wE_x) + r(B_z\mathcal{P}_{yz} + B_y\mathcal{P}_{xx} - B_y\mathcal{P}_{zz} - B_x\mathcal{P}_{xy}) \\ 2r\rho vE_y + 2r(B_x\mathcal{P}_{yz} - B_z\mathcal{P}_{xy}) \\ r\rho(vE_z + wE_y) + r(B_y\mathcal{P}_{xy} - B_z\mathcal{P}_{xz} + B_x\mathcal{P}_{zz} - B_x\mathcal{P}_{yy}) \\ 2r\rho wE_z + 2r(B_y\mathcal{P}_{xz} - B_x\mathcal{P}_{yz}) \end{pmatrix}. \tag{26}$$

Fluxes in the y and z direction are obtained by appropriately permuting the subscripts on the various tensors. In these equations, $r \equiv q/m$ is the charge to mass ratio of the particle and $\rho \equiv mn$ is the mass density. Note that there is one such set of equations for *each* of the s plasma species. These $10s$ equations, coupled to Maxwell equations of electromagnetism, Eqns. (2)–(5), are the ten-moment plasma equations.

Collisions

The collisional operator in the Boltzmann equation is specified in various ways. In most fusion plasmas Coulomb collisions are the dominant collisional processes. An expression for the Coulomb collision operator, $(\partial f_a/\partial t)_c = \sum_b C(f_a, f_b)$, for species a, in terms of the Rosenbluth potentials,

$$H_b(\mathbf{v}) = \int \frac{d\mathbf{v}'}{|\mathbf{v} - \mathbf{v}'|} f_b(\mathbf{v}') \tag{27}$$

$$G_b(\mathbf{v}) = \int d\mathbf{v}' |\mathbf{v} - \mathbf{v}'| f_b(\mathbf{v}'), \tag{28}$$

is

$$C(f_a, f_b) = \frac{\gamma_{ab}}{2m_a} \frac{\partial}{\partial v_i} \left[\frac{\partial}{\partial v_j} \left(f_a \frac{\partial^2 G_b}{\partial v_i \partial v_j} \right) - 2 \left(1 + \frac{m_a}{m_b} \right) f_a \frac{\partial H_b}{\partial v_i} \right]. \tag{29}$$

Here, $\gamma_{ab} = q_a^2 q_b^2 \ln\Lambda_{ab}/(4\pi\epsilon_0^2 m_a)$ with $\Lambda_{ab} = 12\pi\epsilon_0 (m_a T_b + m_b T_a)/(m_a + m_b)\lambda_D$ and λ_D is the Deby length $\lambda_D^{-2} = \sum_a n_a q_a^2/(\epsilon_0 T_a)$. Unfortunately, obtaining analytical expressions for moments of the Coulomb collision operator with the tensor products of the velocity vector $\mathbf{v}$ is not possible. Instead one can use the following $(l + 2k)$-th moment defined by Grad

$$nM^{lk}(\mathbf{v}) = \int d\mathbf{v} \mathbf{P}^l(\mathbf{v}) v_T^{2k} L_k^{(l+1/2)}(s^2) f(\mathbf{x}, \mathbf{v}, \mathbf{t}). \tag{30}$$

Here $v_T = (2T/m)^{1/2}$ is the thermal velocity and $\mathbf{s} = \mathbf{v}/v_T$. The rank-$l$ tensor $\mathbf{P}^l$ is determined from the recurrence relation

$$P_{ijk...m}^{l+1}(\mathbf{v}) = v_i P_{jk...m}^l - \frac{v^2}{2l+1} \frac{\partial P_{jk...m}^l}{\partial v_i} \tag{31}$$

with starting condition $\mathbf{P}^0 = 1$. Also, $L_k^{(l+1/2)}$ are the Sonine (associated Laguerre) polynomials. Now one can expand the distribution function as

$$f = \sum_{ij} f^0 \frac{1}{v_T^{(l+2k)} \sigma_k^l} \mathbf{P}^{lk} \cdot \mathbf{M}^{lk} \tag{32}$$

where $\mathbf{P}^{lk} = \mathbf{P}^l(\mathbf{s}) L_k^{(l+1/2)}(s^2)$ and σ_k^l are normalization constants. Linearizing the Coulomb collision operator [7], and using in the Boltzmann equation one can obtain high-order moment fluid equations. Note the problem of closure still remains but is made more systematic in this framework.

Another option, if the gradients in the velocity space are not large, is to approximate the collision operator using a simple Bhatnagar-Gross-Krook (BGK) model as follows

$$J(f) = \left(\frac{\partial f}{\partial t} \right)_c = v(f^0 - f) + \overline{v}(\overline{f^0} - f), \tag{33}$$

where v and $\overline{v}$ are collision frequencies (units of inverse seconds) and f^0 and $\overline{f^0}$ are Maxwellian distribution functions given by

$$f^0 \equiv n \left(\frac{m}{2\pi kT} \right)^{3/2} \exp\left(-\frac{m}{2\pi kT}(\mathbf{v} - \mathbf{u})^2 \right) \tag{34}$$

$$\overline{f^0} \equiv n \left(\frac{m}{2\pi k\overline{T}} \right)^{3/2} \exp\left(-\frac{m}{2\pi k\overline{T}}(\mathbf{v} - \overline{\mathbf{u}})^2 \right). \tag{35}$$

Here $\overline{T}$, $\overline{\mathbf{u}}$ are relaxed temperatures and bulk velocities. For electron-ion plasma there are four collision frequencies v_e, $\overline{v}_e$ which represent electron-electron and electron-ion collisions and v_i, $\overline{v}_i$ which represent ion-ion and ion-electron collisions. Further, there are eight undetermined parameters $\overline{T}_e$, $\overline{T}_i$ and $\overline{\mathbf{u}}_e$ and $\overline{\mathbf{u}}_i$. Not all of these are independent as the total momentum and energy must be conserved by the collisions.

The advantage of the simple BGK model is that moments of the collision operator with 1, mv_j, $m v_j v_k$ are simple to compute. We get

$$R_c = m \int v_j J(f) d\mathbf{v} = mn\overline{v}(u_j - \overline{u}_j) \tag{36}$$

and

$$P_c = m \int v_j v_k J(f) d\mathbf{v} = v(p\delta_{jk} - P_{jk}) + \overline{v}(\overline{p}\delta_{jk} - P_{jk}) + mn\overline{v}(\overline{u}_j \overline{u}_k - u_j u_k), \tag{37}$$

where the scalar pressure is $p \equiv P_{ii}/3$. From these expressions it is clear that the collisions between like particles do not change momentum but have the effect of driving the off-diagonal terms of the pressure tensor to zero as $1/v \to 0$. By selecting the collision frequencies properly the collisional relaxation of the fluids to a Maxwellian is described sufficiently accurately.

Without extensive calculations it is not possible to evaluate the merits of using a linearized Coulomb collision operator over the simple BGK operator. The choice of a collision operator also affects the closure relations for the heat flux tensor. These issues are being pursued in our current research.

Ten-moment Riemann Problem

The one dimensional *Riemann problem* is a Cauchy problem for the conservation law Eq. 24 with initial

conditions $\mathbf{q}(x < 0,0) = \mathbf{q}_l$ and $\mathbf{q}(x > 0,0) = \mathbf{q}_r$, where $\mathbf{q}_{l,r}$ are constant vectors. Although artificial from a physical standpoint it is fundamental from a mathematical standpoint as its solution illustrates the mathematical structure of hyperbolic balance laws. Solutions to the Riemann problem for the ten-moment equations are presented in this section. The numerical method used is not described but is an extension of the one described in [5]. The Riemann problem selected is a generalization of the Brio-Wu shock-tube problem[2] commonly used to benchmark MHD codes. The initial conditions used are [5, 14]

$$
\begin{bmatrix} \rho_e \\ u_e \\ v_e \\ w_e \\ p_e \\ \rho_i \\ u_i \\ v_i \\ w_i \\ p_i \\ B_x, \\ B_y, \\ B_z, \\ E_x, \\ E_y, \\ E_z \end{bmatrix}_l = \begin{bmatrix} 1.0\frac{m_e}{m_i} \\ 0 \\ 0 \\ 0 \\ 5 \times 10^{-5} \\ 1.0 \\ 0 \\ 0 \\ 0 \\ 5 \times 10^{-5} \\ 0.75 \\ 1.0 \\ 0 \\ 0 \\ 0 \\ 0 \end{bmatrix} \quad \begin{bmatrix} \rho_e \\ u_e \\ v_e \\ w_e \\ p_e \\ \rho_i \\ u_i \\ v_i \\ w_i \\ p_i \\ B_x, \\ B_y, \\ B_z, \\ E_x, \\ E_y, \\ E_z \end{bmatrix}_r = \begin{bmatrix} 0.125\frac{m_e}{m_i} \\ 0 \\ 0 \\ 0 \\ 5 \times 10^{-6} \\ 0.125 \\ 0 \\ 0 \\ 0 \\ 5 \times 10^{-6} \\ 0.75 \\ -1.0 \\ 0 \\ 0 \\ 0 \\ 0 \end{bmatrix} \quad (38)
$$

where $m_e/m_i = 1/1832.6$. Note that the initial pressure tensor is assumed to be isotropic, i.e. $P_{xx} = P_{yy} = P_{zz} = p$ with all other components being set to zero. Simulations with $q_i/m_i = 1, 10$ were carried out. These correspond to skin-depths of 1 and 1/10 respectively. With decreasing skin-depth the solutions tend towards the ideal MHD limit. The solutions were computed on a grid of 5000 cells. All collisional terms were set to zero.

Electron and ion number density at $t = 10$ are show in Fig. 1. The results are significantly different when compared to ideal MHD results and five-moment two-fluid results (see Figs. 1, 2 and 3 in [5]). This is not surprising as the ten-moment model includes more physics than ideal MHD or five-moment models. Also, in absence of collisions the ten-moment model is fundamentally different that the five-moment model, the latter being a fully relaxed limit of the former. In fact, including the BGK collision terms in the simulation and varying the collision frequency drives the solution of the ten-moment equations to that of the two-fluid equations.

Small scale dispersive waves are visible in the solutions. The source terms in the ten-moment (as in the five-moment) model cause the dispersion. To see this we can
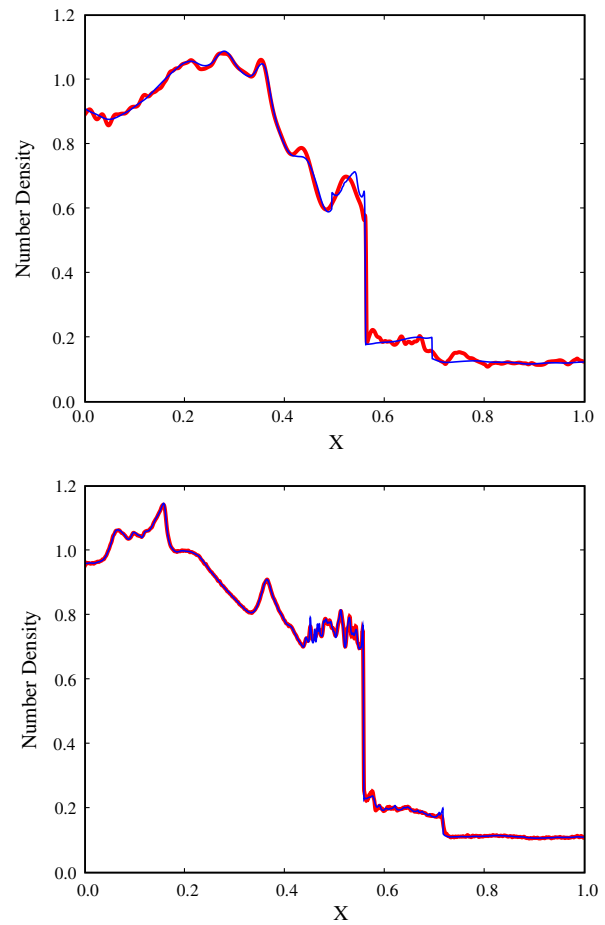

Fig. 1 Electron (thick line) and ion number density (thin line) for ion skin-depth of 1 (top) and 1/10 (bottom) respectively. The results differ significantly from ideal MHD[5] as more physics is included in the ten-moment model. Dispersive wave propagation is clearly visible in the small scale oscillations in the solutions

linearize the conservation law Eq. (24), after writing it in non-conservative form,

$$
\frac{\partial \mathbf{v}}{\partial t} + \mathbf{A}_p \frac{\partial \mathbf{v}}{\partial x} = \mathbf{s}_p, \quad (39)
$$

about a uniform equilibrium $\mathbf{v}_0$. Let $\mathbf{v} = \mathbf{v}_0 + \mathbf{v}_1$, where $\mathbf{v}_1$ is a small perturbation. Using a Taylor series expansion to first-order to write $\mathbf{s}_p(\mathbf{v}) = \mathbf{s}_p(\mathbf{v}_0) + (\partial \mathbf{s}_p/\partial \mathbf{v})_{\mathbf{v}_0} \mathbf{v}_1$ and $\mathbf{A}_p(\mathbf{v}) = \mathbf{A}_p(\mathbf{v}_0) + (\partial \mathbf{A}_p/\partial \mathbf{v})_{\mathbf{v}_0} \mathbf{v}_1$ and letting $\mathbf{M}_p \equiv \partial \mathbf{s}_p/\partial \mathbf{v}$, the linear form of the non-conservative equation, Eq. (36), becomes

$$
\frac{\partial \mathbf{v_1}}{\partial t} + \mathbf{A}_p(\mathbf{v}_0) \frac{\partial \mathbf{v_1}}{\partial x} = \mathbf{M}_p(\mathbf{v}_0) \mathbf{v}_1. \quad (40)
$$

To understand the mathematical structure of the linear equation a Fourier representation of the solution is assumed and each mode is represented as $\mathbf{v}_1 = \hat{\mathbf{v}}_1 e^{i\omega t} e^{ikx}$. Using this in Eq. 40 we obtain

$$\left[i\omega\mathbf{I} + ik\mathbf{A}_p(\mathbf{v}_0) - \mathbf{M}_p(\mathbf{v}_0)\right]\mathbf{v}_1 = 0, \tag{41}$$

where $\mathbf{I}$ is a unit matrix. For non-trivial solutions the determinant of the matrix in the square brackets must vanish, a condition which leads to the dispersion relation $\omega = \omega(k)$. If for all k real, $\omega(k)$ is also real then the linear solutions are undamped. It can be shown that the dispersion relation for the various two-fluid models (five- and ten-moment) in the absence of collisions is nonlinear (as the matrix $\mathbf{M}_p$ is in general non-zero) and non-dissipative. The non-linear dispersion relation indicates dispersion of the waves as they propagate in the plasma. These dispersive effects can also be reproduced in simpler model problems in which the matrix $\mathbf{M}_p$ has purely imaginary eigenvalues. Finding the dispersion relation is equivalent to finding the eigenvalues of the matrix $-k\mathbf{A}_p(\mathbf{v}_0) - i\mathbf{M}_p(\mathbf{v}_0)$. Thus if $\lambda^p(k,\mathbf{v}_0)$ is the pth eigenvalue of this matrix then the pth branch of the dispersion relation is $\omega = \lambda^p(k,\mathbf{v}_0)$. An example of the full ten-moment dispersion relation for perpendicular (to the magnetic field) propagation in a background plasma with a normalized plasma frequency, $\omega_p = 1$, normalized cyclotron frequency, $\omega_c = 0.75$, and normalized thermal velocity, $v_T = 0.447214$, is shown in Fig. 2. In contrast, waves propagate without dispersion for the ideal MHD equations linearized around a uniform plasma.

Fast Magnetic Reconnection

In this section the ten-moment model is applied to simulating fast magnetic reconnection, i.e. the process in which
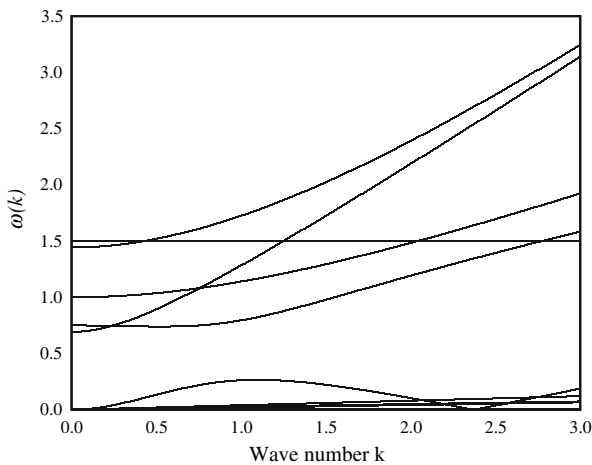

Fig. 2 Scatter plot of the full dispersion relation of the ten-moment model. Note the complex structure of the various branches of the dispersion relation. Some waves in the ten-moment equations suffer a cut-off at a particular wave number but start propagating again without dispersion for larger wave numbers

the topology of the magnetic field lines changes violently [12]. For this problem we have ignored all collision terms in the ion equations and set the heat flux tensor to zero. Further, we have assumed that the electron-electron collisions are sufficient to drive the off-diagonal terms of the electron pressure tensor to zero (i.e. the electrons are fully relaxed). In this case the electron fluid is described by just five equations (continuity, momentum and total energy equations). Ignoring ion collisions is appropriate for this problem as the time scale of fast magnetic reconnection is much faster than ion relaxation time scale. Further, the bulk reconnection rate, although much faster than that described by resistive MHD, is not dependent on collisions. In ideal MHD or ideal Hall MHD the field line topology cannot change, i.e. the field lines are "frozen" into the fluid (frozen into the electron fluid in case of ideal Hall-MHD). The situation is analogous to neutral ideal fluid flow in which vortex tube topology remains constant. Even small resistivity (viscosity in neutral fluids), however, can make the topology change and the field lines reconnect and this process is adequately described in the framework of resistive MHD or Hall-MHD. In a low collisionality plasma magnetic reconnection is also observed to occur and at a much faster rate than in collisional plasmas. Fast collisionless reconnection is important in understanding many space plasma phenomena, for example, solar flares and the dynamics of the Earth's magnetotail during a geomagnetic substorm. It also occurs during formation of an FRC from theta-pinch reversal. To understand the mechanism of fast reconnection a number of plasma models were used to study reconnection of oppositely directed magnetic fields separated by a thin current sheet. This was the Geospace Environmental Modeling (GEM) Reconnection Challenge [3]. The various models used were electron MHD [6], Hall MHD with anisotropic pressure [1], MHD and Hall MHD [9, 10, 13], full particle [11] and hybrid [8] models. It was found that the although reconnection initiates at length scales on the order of the electron skin depth the reconnection rate is governed by ion dynamics. The ten-moment model can describe the physics at electron skin depth scales as well as full ion dynamics and hence can describe fast reconnection correctly. On the electron-skin depth scales the field lines are no longer frozen to the electron fluid and this allows the reconnection to initiate without the need for resistivity. On the other hand in the Hall MHD model [9] the reconnection needs to be initiated by using a small resistivity.

The simulation is initialized with oppositely directed magnetic fields separated by a thin current sheet. The magnetic field is given by

$$\mathbf{B}(y) = B_0 \tanh(y/\lambda)\mathbf{e}_x. \tag{42}$$

The initial current is carried only by the electrons:

$$\mathbf{J}_e = -\frac{B_0}{\lambda}\operatorname{sech}^2(y/\lambda). \tag{43}$$

The number densities of the ions and electrons are initialized as $n_e(y) = n_i(y) = n(y)$, where

$$n(y) = n_0\big(1/5 + \operatorname{sech}^2(y/\lambda)\big). \tag{44}$$

The electron pressure is set to $p_e(y) = p(y)$ and ion pressure to $p_i(y) = 5p(y)$ where

$$p(y) = \frac{B_0}{12}n(y). \tag{45}$$

To initiate reconnection in a controlled manner the magnetic field is perturbed with $\delta\mathbf{B} = \mathbf{e}_z \times \nabla\psi$, where

$$\psi(x,y) = \psi_0 \cos(2\pi x/L_x)\cos(\pi y/L_y), \tag{46}$$

and $[-L_x/2, L_x/2] \times [-L_y/2, L_y/2]$ is the simulation domain. This form of the perturbation assures that $\nabla \cdot \mathbf{B} = 0$ at $t = 0$. Periodic boundaries are applied at $x = \pm L_x/2$ and open boundaries at $y = \pm L_y/2$. Simulations presented below are for a 256×128 grid. The other parameters used are $m_e/m_i = 1/25$, $L_x = 8\pi$, $L_y = 4\pi$, $\psi_0 = B_0/10$ and $\lambda = 0.5$. The unit length scale is the ion skin-depth and the unit time scale is in inverse ion cyclotron frequency. These parameters are similar to the original GEM challenge problem.

To compare results with the models used in the GEM challenge problem the reconnected flux, ϕ, was computed using

$$\phi(t) = \frac{1}{2L_x}\int_{-L_x/2}^{L_x/2}|B_y(x, y = 0, t)|\,dx. \tag{47}$$

As the reconnection proceeds the reconnected flux, which is a measure of the net Y-direction magnetic field, increases and indicates the reconnection rate. Figure 3 shows the reconnected flux history. It is observed that the reconnection occurs at about $t = 10$ and the reconnected flux increases rapidly after that. The computed flux history is in excellent agreement with flux histories from full particle and hybrid models used in the original GEM Challenge problem. Figure 4 shows the electron and ion number densities at $t = 25$. Counter-streaming fluid instabilities are excited at later times due to the strong electron flow at the edge of the current sheet.

Conclusions

We have presented a high-order moment model for extended MHD simulations. The model includes electron
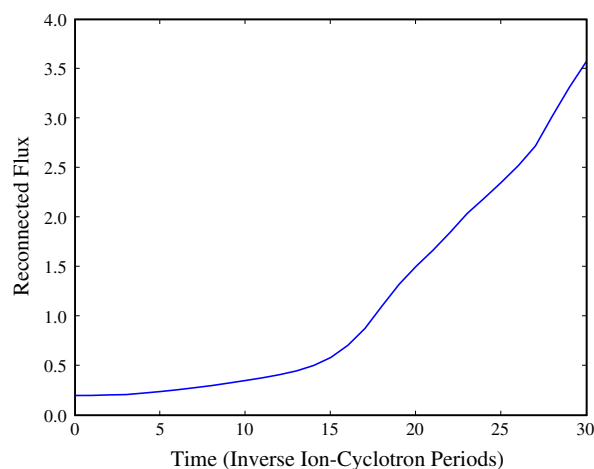

Fig. 3 Reconnected flux from the ten-moment model. Time measured in ion-cyclotron periods is plotted on the X-axis and reconnected flux on the Y-axis. The reconnection rate obtained here agrees well with the two-fluid results presented in [5]
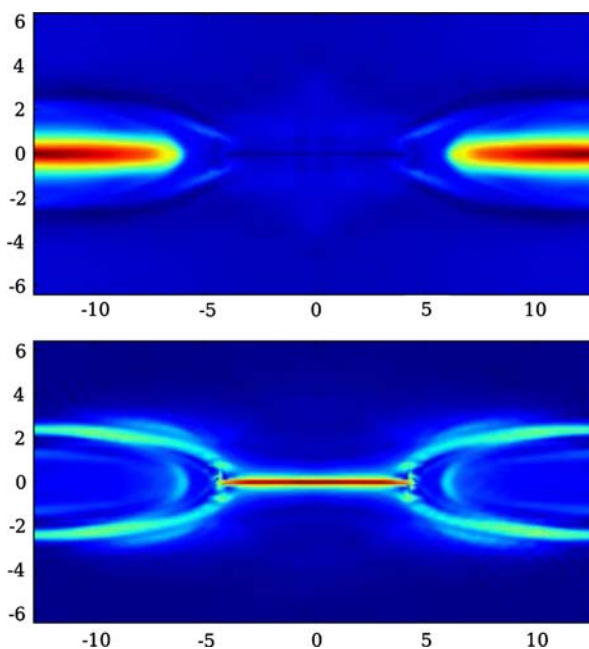

Fig. 4 Electron number density (top) and current density (bottom) at $t = 25$. The reconnection process is well under way by this time. The electrons show a strong flow at the edge of the sheet which eventually leads to counter streaming fluid instabilities

inertia, displacement currents, non-neutral effects and finite Larmor radius (FLR) effects. The model is validated using the well known GEM fast magnetic reconnection problem. Correct reconnection rates are obtained hence validating the model.

The results presented here are preliminary and several directions of research are being pursued. In particular the effects of collisions are being incorporated. Initially the

simple Bhatnagar-Gross-Krook (BGK) model is being used to study relaxation of the distribution function to a Maxwellian. The use of the exact linearized Coulomb collision operator [7] as outlined above is also being explored. The problem of closure is a complex one and depends on the form of the collision operator used and often on the particular physical situation being studied. For the ten-moment model it seems natural that Chapman-Enskog type expansion be carried out about the Gaussian distribution (see Eq. 23) rather than the Maxwellian. This allows arbitrary anisotropy in the pressure tensor without the distribution function going negative. A unexplored question is the incorporation of linear Landau damping effects in the fluid closures. Incorporating Landau damping in collisional plasmas is not simple and will be explored in the future. The ten-moment and five-moment models are being used to study Field Reversed Configuration (FRC) formation and stability in full three dimensions. It is expected that the additional inclusion of the FLR effects in the ten-moment model, coupled to an appropriate closure for the heat-flux tensor, will lead to an understanding of FRC stability.

References

1. J. Birn, M. Hesse, J. Geophys. Res. **106**(A3), 3737 (2001)
2. M. Brio, C.C. Wu, J. Comput. Phys. **75**, 400–422 (1988)
3. J. Birn et al., J. Geophys. Res. **106**, 3715 (2001)
4. J.P. Friedberg, *Ideal Magnetohydrodynamics*. (Plenum Press, 1987)
5. A. Hakim, J. Loverich, U. Shumlak, J. Comput. Phys. **219**, 418–442 (2006)
6. M. Hesse, J. Birn, M. Kuznetsova, J. Geophys. Res. **106**(A3), 3721 (2001)
7. J.-Y. Ji, E.D. Held, Phys. Plasma. **13**, 102103 (2006)
8. M.M. Kuznetsova, M. Hesse, D. Winske, J. Geophys. Res. **106**(A3), 3799 (2001)
9. Z.W. Ma, A. Bhattacharjee, J. Geophys. Res. **106**(A3), 3773 (2001)
10. A. Otto, J. Geophys. Res. **106**(A3), 3751 (2001)
11. P.L. Prichette, J. Geophys. Res. **106**(A3), 3783 (2001)
12. P. Eric, F. Terry, *Magnetic Reconnection*. Cambridge University Press (2000)
13. M.A. Shay, J.F. Drake, B.N. Rogers, R.E. Denton, J. Geophys. Res. **106**(A3), 3759 (2001)
14. U. Shumlak, J. Loverich, J. Comput. Phys. **187**, 620–638 (2003)